

Non-Gaussian quantum states of a multimode light field

Young-Sik Ra,^{1,2,*} Adrien Dufour,¹ Mattia Walschaers,¹
Clément Jacquard,¹ Thibault Michel,^{1,3} Claude Fabre,¹ and Nicolas Treps¹

¹*Laboratoire Kastler Brossel, UPMC-Sorbonne Universités, CNRS,
ENS-PSL Research University, Collège de France; 4 place Jussieu, 75252 Paris, France*

²*Department of Physics, Korea Advanced Institute of Science and Technology (KAIST), Daejeon 34141, Korea*

³*Center for Quantum Computation and Communication Technology, Department of Quantum Science,
The Australian National University, Canberra, ACT 0200, Australia*

(Dated: December 21, 2021)

Even though Gaussian quantum states of multimode light are promising quantum resources due to their scalability, non-Gaussianity is indispensable for quantum technologies, in particular to reach quantum computational advantage. However, embodying non-Gaussianity in a multimode Gaussian state remains a challenge as controllable non-Gaussian operations are hard to implement in a multimode scenario. Here, we report the first generation of non-Gaussian quantum states of a multimode light field by subtracting a photon in a desired mode from multimode Gaussian states, and observe negativity of the Wigner function. For entangled Gaussian states, we observe that photon subtraction makes non-Gaussianity spread among various entangled modes. In addition to applications in quantum technologies, our results shed new light on non-Gaussian multimode entanglement with particular emphasis on quantum networks.

Advanced quantum technologies require scalable and controllable quantum resources [1, 2]. Gaussian states of multimode light such as squeezed states and cluster states are scalable quantum systems [3–5], which can be generated on demand. However, non-Gaussian features are indispensable in many quantum protocols, especially to reach a quantum computation advantage [6]. Embodying non-Gaussianity in a multimode quantum state remains a challenge as non-Gaussian operations generally cannot maintain coherence among multiple modes [7]. Here, we generate non-Gaussian quantum states of a multimode light field, and observe negativity of the Wigner function in adjustable modes. For this purpose, starting from the deterministic generation of Gaussian entangled states, we use sum-frequency generation to remove a single photon in a computer-controlled coherent superposition of optical modes. We reveal the induced non-Gaussian features and observe how they spread among the entangled modes, depending on the mode in which the photon is subtracted. The resulting non-Gaussian multimode quantum states will have broad applications for universal quantum computing [8, 9], entanglement distillation [10], and a nonlocality test [11].

Our starting point is a squeezed vacuum state of light, a basic quantum resource for continuous-variable quantum technologies such as quantum-enhanced sensing [12], deterministic quantum state teleportation [13], and measurement-based quantum computing [9]. Recent technological advances have extended the generation and

control of squeezed vacuum from a single mode to multiple modes, which enables a deterministic generation of large-scale multipartite entangled states [3–5]. However, such quantum states are intrinsically Gaussian states, which always exhibit Gaussian statistics in electric field quadrature measurements. These states have limitations on quantum applications, e.g., universal quantum computing [8, 9] and entanglement distillation [10]. In particular, the ability to produce a non-Gaussian quantum state is essential to reach quantum advantages [6], which is connected to exotic quantum features of non-Gaussian quantum states. The most profound example thereof is contextuality, which goes hand in hand with negative values of the Wigner function [14]. Another example is multimode entanglement, which can have conceptually different properties in non-Gaussian states as compared with their Gaussian counterparts [15].

The hybrid approach, which combines continuous-variable and discrete-variable quantum information processing, provides a solution [1]. Subtracting/adding a discrete number of photons [16] or coupling with a discrete-level quantum system [17] can generate non-Gaussian states such as a local or non-local superposition of coherent states [18–20] and hybrid entanglement [21, 22]. Hitherto, this approach has only been successfully applied to a single- or two-mode quantum state, and the extension to highly multimode quantum states remains challenging due to the arduous task of maintaining coherence among multiple modes. For example, the conventional method of photon subtraction for a single-mode quantum state is based on a simple beam splitter [16]; when applied to a multimode quantum state, however, the method results in the generation of a mixed quantum state [7].

To exploit the full potential of the large-scale entangled states available in the continuous-variable quantum information processing [3–5], it is essential that the hybrid approach is made compatible with multimode quantum

* youngsikra@gmail.com

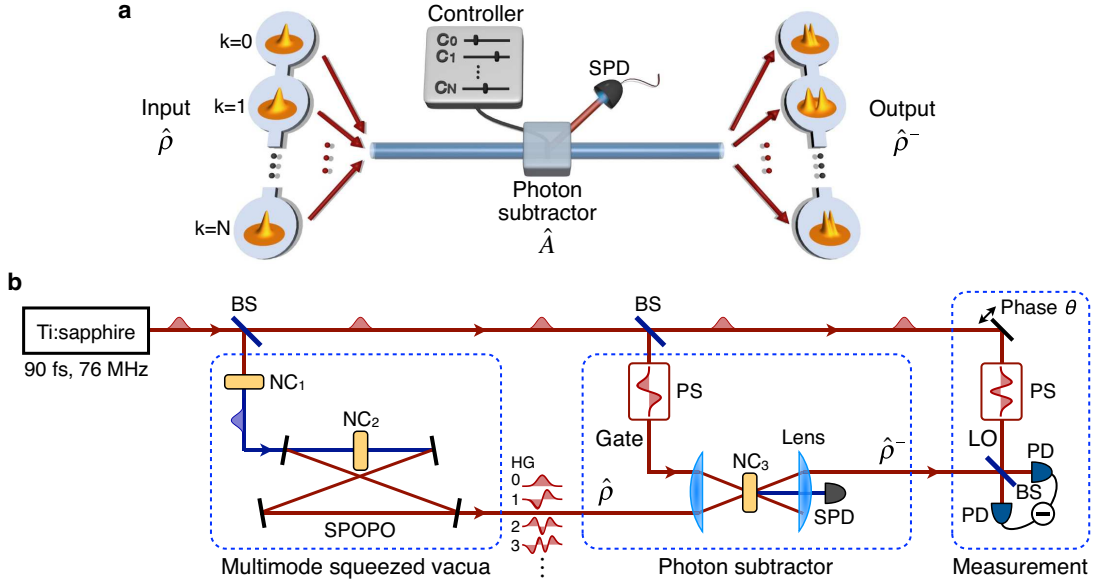


FIG. 1. **Mode-selective photon subtraction from a multimode quantum state.** (a) Concept. Input is a beam containing a Gaussian multimode quantum state $\hat{\rho}$, which can be, in general, a multipartite entangled state. From the input state, we subtract a photon in a specific mode or in a coherent superposition of multiple modes by controlling the complex coefficient c_k for each mode k . This process, described by an annihilation operator \hat{A} in Eq. (1), is heralded by a registration of a photon at the single-photon detector (SPD). As a result, the output beam contains a non-Gaussian multimode quantum state $\hat{\rho}^-$. The inset inside each circle is the Wigner function of the reduced quantum state in the associated mode. (b) Experimental setup. A Ti:sapphire laser produces a beam made of a train of femtosecond pulses, which splits into three beams. One beam is up-converted via second harmonic generation in a second-order nonlinear crystal (NC₁), and then, pumps NC₂ for a parametric down-conversion process. Synchronously pumped optical parametric oscillator (SPOPO) amplifies the process, which generates twelve-mode squeezed vacua in well-defined time-frequency modes. Another beam is used as a gate for the photon subtractor, and its time-frequency mode is engineered by a pulse shaper (PS). Inside NC₃, sum-frequency-interaction between the gate and the multimode squeezed vacua generates an up-converted beam, which is detected by SPD. A photon registration in SPD heralds photon subtraction from the multimode squeezed vacua. The resulting multimode quantum state is measured by homodyne detection with a time-frequency-engineered local oscillator (LO) using another PS. PD: photo diode; BS: beam splitter; θ : phase of LO.

states, e.g., via photon subtraction operating in multiple modes coherently. The concept of our experiment is illustrated in Fig. 1(a). If we call $\hat{\rho}$ the density operator of an input multimode quantum state, the output state $\hat{\rho}^-$ by a photon subtraction operator \hat{A} becomes

$$\hat{\rho}^- \propto \hat{A} \hat{\rho} \hat{A}^\dagger, \quad \text{where } \hat{A} = \sum_{k=0} c_k \hat{a}_k. \quad (1)$$

c_k are complex numbers normalized as $\sum |c_k|^2 = 1$, and \hat{a}_k is the annihilation operator for mode k . Note that \hat{A} is, in general, a coherent superposition of annihilation operators in multiple modes. The ability to experimentally control both the c_k coefficient and the multimode resource $\hat{\rho}$ is the key to tailor non-Gaussian multimode states and to achieve non-Gaussian entanglement for building non-Gaussian quantum networks [23, 24].

In our experiment, the controlled generation of non-Gaussian multimode quantum states is performed using quantum frequency combs as a resource. Figure 1(b) shows the experimental setup, whose details are presented in Methods. The optical modes in which we implement Eq. (1) are time-frequency modes [25]. The in-

terest of these modes is that they are co-propagating in the same transverse mode, allowing for a large multimode quantum resource to keep its coherence and to access arbitrary superpositions of modes through elaborate techniques in ultrafast optics. We populate these modes with a highly multimode Gaussian state through a parametric down conversion process [4]. Tailoring the measurement mode basis allows for the generation of versatile multipartite entangled states [26]. We combine this resource with a time-frequency mode-dependent photon subtractor to de-Gaussify such multimode Gaussian states.

More specifically, our multimode Gaussian resource $\hat{\rho}$ is a set of independent squeezed vacua whose eigen modes are conveniently approximated by Hermite-Gaussian modes HG_k . In order to implement the concepts of Eq. (1), we associate these modes with the annihilation operators \hat{a}_k . Hence, it remains to control the c_k coefficients for the photon subtraction. As shown in Fig. 1(b), this is implemented through a mode-selective sum-frequency generation between the Gaussian resource $\hat{\rho}$ and a gate beam [27]. The non-linear interaction is designed such that pulse-shaping the gate allows for the

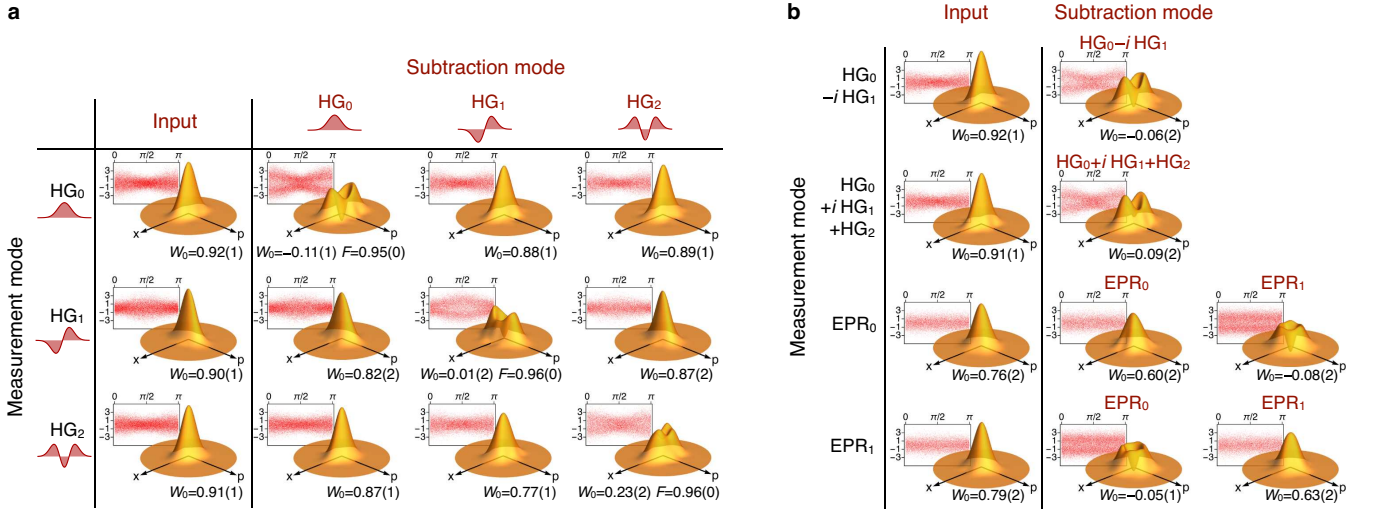


FIG. 2. **Wigner function reconstructed from experimental data.** For a multimode quantum state, photon subtraction and measurement are conducted in (a) HG modes or in (b) superpositions of HG modes. The Wigner function of each mode is represented in the phase space of x and p axes, which are associated with quadrature operators $\hat{x} = \hat{a} + \hat{a}^\dagger$ and $\hat{p} = (\hat{a} - \hat{a}^\dagger)/i$, respectively. The inset behind each Wigner function shows the experimentally obtained quadrature outcomes, where the horizontal and vertical axes represent the phase of local oscillator and a quadrature outcome, respectively; the quadrature outcome of one corresponds to the variance of the vacuum fluctuation. No correction of optical losses is made; for the results by optical loss correction, see Extended Data Fig. 1. $W_0 = 2\pi W(0, 0)$ is the value of a normalized Wigner function at the origin, and F is the fidelity between an experimental Wigner function and the Wigner function by the ideal photon subtraction to the input state of the corresponding mode. Purities of the Wigner functions in (a), compared with the cases of the ideal photon subtraction, are presented in Extended Data Tab. 1. For measurements in modes EPR_0 and EPR_1 , the phase of a quadrature outcome is randomized since the associated quantum state is phase insensitive. Errors noted in parentheses are 1 s. d.

control of the mode of photon subtraction [25]. Finally, detection of a single photon in the up-converted beam heralds the subtraction of a photon in the desired mode from the Gaussian resource.

In practice, in order to implement the operator \hat{A} , the mode of the gate should be set as $v_g = \sum_k (-1)^k c_k \text{HG}_k$ [27], which is efficiently performed using a computer controlled pulse shaper. The intensity of the gate governs the efficiency of the operation, and hence the heralding probability. To characterize the generated non-Gaussian multimode quantum state, we employ a homodyne detection that can control the mode of measurement by pulse-shaping the local oscillator.

We first measure the input multimode squeezed vacua without photon subtraction (i.e., no gate field is applied). As expected, the measured state exhibits Gaussian distribution: see the input Wigner functions shown in the first column of Fig. 2(a). On the other hand, when a single photon is subtracted in HG_0 (the second column), we observe that the Wigner function in HG_0 becomes non-Gaussian while the Wigner functions in the other modes remain Gaussian. This result shows the mode-selective operation of the photon subtractor necessary for multimode quantum states. The non-Gaussian Wigner function in HG_0 exhibits a negative value at the origin (W_0), as is required to achieve quantum advantages [6], and the negativity indicates a negative value in the entire multimode Wigner function (see Methods). When a photon

is subtracted in HG_1 (HG_2), we similarly observe a non-Gaussian Wigner function only in HG_1 (HG_2). Compared with the photon subtraction in HG_0 , photon subtraction in the higher order modes results in a less non-Gaussian Wigner function. This is mainly because the input state in a higher order mode has a larger optical loss than HG_0 : we have found a high fidelity (F) between a non-Gaussian Wigner function obtained in experiment with the ideal Wigner function calculated by subtracting a photon from the corresponding input state.

Furthermore, the versatility of the experimental setup allows for the computer controlled subtraction of a photon in an arbitrary superposition of modes from a multimode quantum state. As an example, we subtract a photon in a superposition of HG_0 and HG_1 modes, $\text{HG}_0 - i\text{HG}_1$ [28]. We now observe a non-Gaussian Wigner function in this mode (first row of Fig. 2(b)). On the other hand, in the orthogonal mode $\text{HG}_0 + i\text{HG}_1$, a Gaussian Wigner function is obtained, and in a partially overlapping mode $i\text{HG}_1$, an intermediate situation is obtained as expected, see Extended Data Fig. 2. When we subtract a photon in a superposition of three modes $\text{HG}_0 + i\text{HG}_1 + \text{HG}_2$, we similarly observe a non-Gaussian Wigner function in the same superposed modes (second row of Fig. 2(b)).

This flexibility of the setup allows us to extend photon subtraction to entangled input states. We first investigate an Einstein-Podolsky-Rosen (EPR) entan-

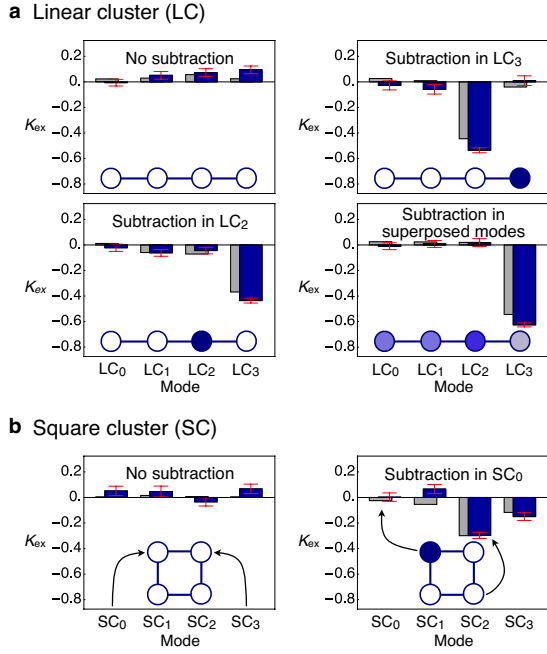


FIG. 3. **Effect of photon subtraction on cluster states.** (a) A linear and (b) a square cluster state. K_{ex} , defined in Eq. (2), is the excess kurtosis of quadrature outcomes by randomizing the phase information, where $K_{\text{ex}} < 0$ indicates a non-Gaussian quantum state. For the photon subtraction in the superposed modes (bottom right in (a)), we use $-0.4iLC_0 - 0.4LC_1 + 0.8iLC_2 + 0.2LC_3$. Blue and gray bars are experimental and theoretical values, respectively. The theoretical model is described in Methods. Error bars for experimental data are 1 s. d.

gled state, which exhibits quantum correlations between two superposed modes: $\text{EPR}_0 = \text{HG}_0 + \text{HG}_1$ and $\text{EPR}_1 = \text{HG}_0 - \text{HG}_1$ (see Methods). The last two rows in Fig. 2(b) show the experimentally obtained Wigner functions. Without photon subtraction, the reduced quantum state in each of EPR_0 and EPR_1 is a thermal state as expected. When a photon is subtracted in EPR_0 , the introduced non-Gaussian characteristic appears in the other mode (EPR_1) with almost no effect on the mode in which the photon is actually subtracted, and vice versa. In striking contrast with the aforementioned separable input state, the effect of photon subtraction on an entangled state is not localized but is transferred to another mode.

To open genuine perspectives for applications in quantum technologies, we show the scalability of our approach to larger multimode entangled states. We consider a four-mode linear cluster (LC) state and a four-mode square cluster (SC) state (see Methods), where we denote the four modes of the linear one as LC_k ($k = 0, 1, 2, 3$) and the square one as SC_k ($k = 0, 1, 2, 3$). Due to the large dimension of the state, full tomography becomes impractical. Thus, we quantify the non-Gaussianity in each mode by evaluating the phase-averaged excess kurtosis (to compare with the kurtosis of 3 by a Gaussian dis-

tribution). This is obtained from the quadrature measurement outcomes x_1, x_2, \dots, x_S where the measurement phase is randomized:

$$K_{\text{ex}} = \frac{\frac{1}{S} \sum_{s=1}^S x_s^4}{\left(\frac{1}{S} \sum_{s=1}^S x_s^2\right)^2} - 3 \quad (2)$$

For a quantum state with zero mean ($\langle \hat{a} \rangle = \langle \hat{a}^\dagger \rangle = 0$), which corresponds to all the quantum states in our experiment, a Gaussian state always exhibits $K_{\text{ex}} \geq 0$, thus $K_{\text{ex}} < 0$ indicates a non-Gaussian state. Figure 3 shows excess kurtosis of the generated states. For the linear cluster state, excess kurtosis in each mode is initially close to zero. When a photon is subtracted in LC_3 , it is LC_2 in which excess kurtosis becomes highly negative (i.e. non Gaussian) while those in the other modes remain close to 0. For photon subtraction in LC_2 , only LC_3 exhibits a significant negativity. We can concentrate more non-Gaussianity in LC_3 by subtracting a photon in a superposition of four modes, as shown in the last figure of Fig. 3(a). For the square cluster state, excess kurtosis without photon subtraction is close to zero in each mode. Photon subtraction in SC_0 , however, does not affect the distributions in its nearby modes (SC_1 and SC_3) much, but it introduces non-Gaussianity mostly in SC_2 which is two steps away from the mode of photon subtraction.

We have generated non-Gaussian quantum states of a multimode light by subtracting a photon from multimode Gaussian states. The selectivity and the controllability of the mode(s) for the photon subtraction make it possible to extend the non-Gaussianity of a quantum state to the multimode regime, which has been a main obstacle for scalable quantum information processing [1, 2]. The availability of non-Gaussian multimode states will stimulate fundamental studies on multipartite entanglement [15] and multimode quantumness [29] by going beyond the Gaussian realm, as well as applications in quantum computing [8, 9] and quantum communication [10, 11]. In particular, the observed nontrivial interplay between photon subtraction and cluster states, confirming recent theoretical predictions [24], provides new insights into the fields of quantum networks [30] and quantum transport [31].

ACKNOWLEDGMENTS

This work is supported by the French National Research Agency projects COMB and SPOCQ, the European Union Grant QCUMBER (no. 665148). C.F. and N.T. are members of the Institut Universitaire de France. Y.-S.R. acknowledges support from the European Commission through Marie Skłodowska-Curie actions (no. 708201) and support from Basic Science Research Program through the National Research Foundation of Korea (NRF) funded by the Ministry of Education (2018R1A6A3A03012129). M.W. acknowledges funding

through research fellowship WA 3969/2-1 from the Ger-

man Research Foundation (DFG).

-
- [1] Andersen, U. L., Neergaard-Nielsen, J. S., Van Loock, P. and Furusawa, A., Hybrid discrete- and continuous-variable quantum information, *Nat. Phys.* **11**, 713–719 (2015).
 - [2] Biamonte, J. *et al.*, Quantum machine learning, *Nature* **549**, 195–202 (2017).
 - [3] Yokoyama, S. *et al.*, Ultra-large-scale continuous-variable cluster states multiplexed in the time domain, *Nat. Photonics* **7**, 982–986 (2013).
 - [4] Roslund, J., Medeiros de Araújo, R., Jiang, S., Fabre, C. and Treps, N., Wavelength-multiplexed quantum networks with ultrafast frequency combs, *Nat. Photonics* **8**, 109–112 (2014).
 - [5] Chen, M., Menicucci, N. C. and Pfister, O., Experimental Realization of Multipartite Entanglement of 60 Modes of a Quantum Optical Frequency Comb, *Phys. Rev. Lett.* **112**, 120505 (2014).
 - [6] Mari, A. and Eisert, J., Positive Wigner Functions Render Classical Simulation of Quantum Computation Efficient, *Phys. Rev. Lett.* **109**, 230503 (2012).
 - [7] Averchenko, V., Jacquard, C., Thiel, V., Fabre, C. and Treps, N., Multimode theory of single-photon subtraction, *New J. Phys.* **18**, 083042 (2016).
 - [8] Lloyd, S. and Braunstein, S. L., Quantum computation over continuous variables, *Phys. Rev. Lett.* **82**, 1784–1787 (1999).
 - [9] Menicucci, N. C. *et al.*, Universal quantum computation with continuous-variable cluster states, *Phys. Rev. Lett.* **97**, 110501 (2006).
 - [10] Eisert, J., Scheel, S. and Plenio, M. B., Distilling Gaussian States with Gaussian Operations is Impossible, *Phys. Rev. Lett.* **89**, 137903 (2002).
 - [11] Plick, W. N., Arzani, F., Treps, N., Diamanti, E. and Markham, D., Violating Bell inequalities with entangled optical frequency combs and multipixel homodyne detection, *Phys. Rev. A* **98**, 062101 (2018).
 - [12] Aasi, J. *et al.*, Enhanced sensitivity of the LIGO gravitational wave detector by using squeezed states of light, *Nat. Photonics* **7**, 613–619 (2013).
 - [13] Takeda, S., Mizuta, T., Fuwa, M., Van Loock, P. and Furusawa, A., Deterministic quantum teleportation of photonic quantum bits by a hybrid technique, *Nature* **500**, 315–318 (2013).
 - [14] Spekkens, R. W., Negativity and Contextuality are Equivalent Notions of Nonclassicality, *Phys. Rev. Lett.* **101**, 020401 (2008).
 - [15] Valido, A. A., Levi, F. and Mintert, F., Hierarchies of multipartite entanglement for continuous-variable states, *Phys. Rev. A* **90**, 052321 (2014).
 - [16] Wenger, J., Tualle-Brouiri, R. and Grangier, P., Non-Gaussian statistics from individual pulses of squeezed light, *Phys. Rev. Lett.* **92**, 153601 (2004).
 - [17] Vlastakis, B. *et al.*, Deterministically Encoding Quantum Information Using 100-Photon Schrödinger Cat States, *Science (New York, NY)* **342**, 607–610 (2013).
 - [18] Ourjoumtsev, A., Tualle-Brouiri, R., Laurat, J. and Grangier, P., Generating optical Schrödinger kittens for quantum information processing, *Science (New York, NY)* **312**, 83–86 (2006).
 - [19] Sychev, D. V. *et al.*, Enlargement of optical Schrödinger’s cat states, *Nat. Photonics* **11**, 379–382 (2017).
 - [20] Ourjoumtsev, A., Ferreyrol, F., Tualle-Brouiri, R. and Grangier, P., Preparation of non-local superpositions of quasi-classical light states, *Nat. Phys.* **5**, 189–192 (2009).
 - [21] Jeong, H. *et al.*, Generation of hybrid entanglement of light, *Nat. Photonics* **8**, 564–569 (2014).
 - [22] Morin, O. *et al.*, Remote creation of hybrid entanglement between particle-like and wave-like optical qubits, *Nat. Photonics* **8**, 570–574 (2014).
 - [23] Walschaers, M., Fabre, C., Parigi, V. and Treps, N., Entanglement and Wigner Function Negativity of Multimode Non-Gaussian States, *Phys. Rev. Lett.* **119**, 183601 (2017).
 - [24] Walschaers, M., Sarkar, S., Parigi, V. and Treps, N., Tailoring Non-Gaussian Continuous-Variable Graph States, *Phys. Rev. Lett.* **121**, 220501 (2018).
 - [25] Ansari, V., Donohue, J. M., Brecht, B. and Silberhorn, C., Tailoring nonlinear processes for quantum optics with pulsed temporal-mode encodings, *Optica* **5**, 534–550 (2018).
 - [26] Cai, Y. *et al.*, Multimode entanglement in reconfigurable graph states using optical frequency combs, *Nat. Commun.* **8**, 15645 (2017).
 - [27] Ra, Y.-S., Jacquard, C., Dufour, A., Fabre, C. and Treps, N., Tomography of a Mode-Tunable Coherent Single-Photon Subtractor, *Phys. Rev. X* **7**, 031012 (2017).
 - [28] The normalization constant is omitted for simplicity, and $-i$ is introduced to rotate the x -squeezed vacuum in HG_1 to p -squeezed vacuum such that both HG_0 and HG_1 have a p -squeezed vacuum.
 - [29] Hudson, R. L., When is the wigner quasi-probability density non-negative?, *Rep. Math. Phys.* **6**, 249–252 (1974).
 - [30] Kimble, H. J., The quantum internet, *Nature* **453**, 1023–1030 (2008).
 - [31] Walschaers, M., Schlawin, F., Wellens, T. and Buchleitner, A., Quantum Transport on Disordered and Noisy Networks: An Interplay of Structural Complexity and Uncertainty, *Annu. Rev. Condens. Matter Phys.* **7**, 223–248 (2016).
 - [32] Neergaard-Nielsen, J., Nielsen, B., Hettich, C., Molmer, K. and Polzik, E., Generation of a Superposition of Odd Photon Number States for Quantum Information Networks, *Phys. Rev. Lett.* **97**, 083604 (2006).
 - [33] Duan, L.-M., Giedke, G., Cirac, J. I. and Zoller, P., Inseparability Criterion for Continuous Variable Systems, *Phys. Rev. Lett.* **84**, 2722–2725 (2000).
 - [34] Simon, R., Peres-Horodecki Separability Criterion for Continuous Variable Systems, *Phys. Rev. Lett.* **84**, 2726–2729 (2000).
 - [35] Bowen, W. P., Schnabel, R., Lam, P. K. and Ralph, T. C., Experimental Investigation of Criteria for Continuous Variable Entanglement, *Phys. Rev. Lett.* **90**, 043601 (2003).
 - [36] van Loock, P., Weedbrook, C. and Gu, M., Building Gaussian cluster states by linear optics, *Phys. Rev. A* **76**, 032321 (2007).

I. METHODS

Experimental details. Non-Gaussian multimode quantum states are generated by several nonlinear interactions on femtosecond pulses, as described in Fig. 1. The fundamental light source is a Ti:Sapphire laser, which produces a train of pulses (duration: 90 fs, central wavelength: 795 nm) at a repetition rate of 76 MHz. The laser beam is split into three beams: one is used for generating a multimode Gaussian state, another for photon subtraction, and the third for the homodyne detection.

The first beam is up-converted to a femtosecond pulse having 397.5-nm central wavelength in NC₁ (0.2-mm-thick BiB₃O₆) which is used as a pump for a parametric-down-conversion process in NC₂ (2-mm-thick BiB₃O₆) inside a cavity, the SPOPO. The length of the SPOPO is locked to the length of the Ti-Sapphire laser via the Pound-Drever-Hall method, such that the train of pump pulses is synchronized with the down-converted pulses which circulate inside the SPOPO. Transmittance of the output coupler of the SPOPO is 50%. The light coming out through the output coupler is a multimode Gaussian state, containing roughly twelve squeezed vacua in orthogonal time-frequency modes [4, 26]. Among the twelve modes, we focus on the first four dominating modes, whose covariance matrix is given in Extended Data Fig. 3.

For photon subtraction, we perform sum-frequency interaction between the multimode Gaussian state and the second beam from the Ti-Sapphire laser (the gate; 1 mW power) inside NC₃ (2.5-mm-thick BiB₃O₆). Detection of a single photon generated by the sum-frequency interaction heralds photon subtraction from the multimode squeezed vacua, where the time-frequency mode of the gate determines the photon subtraction mode [27]. To engineer the time-frequency mode of the gate, we employ a homemade pulse shaper whose core element is a spatial light modulator, having a spectral resolution of 0.2 nm. Conversion efficiency of the nonlinear interaction is 0.1 %, and we have typically 110 Hz of heralding rate with background noise of 6 Hz.

The last beam is used as the local oscillator (LO) of the homodyne detection to measure the generated quantum state. The measurement mode is the mode of the LO, which is engineered by another pulse shaper having a spectral resolution of 0.2 nm. For each event of photon subtraction, photocurrent difference between the two PDs is sampled every 2 ns during a 2- μ s time window, and one quadrature outcome is obtained by calculating the dot product between the samples and the double-sided-decaying-shape temporal mode of the SPOPO [32]. To reconstruct a Wigner function in Fig. 2, we collect 20,000 \sim 30,000 quadrature outcomes. In the case of no photon subtraction, we monitor the variance of the quadrature outcomes. Phase dependence of the quadrature squeezing of the multimode Gaussian state provides the phase information of the LO relative to this multimode light.

Preparation of entangled states. We prepare an entangled state by choosing a specific basis of modes in which quantum correlations among desired modes emerge [4, 26]. In the HG mode basis, even-order (odd-order) modes exhibit p -quadrature (x -quadrature) squeezed vacuum. To prepare an EPR entangled state, we use a basis of $\text{EPR}_0 = \frac{1}{\sqrt{2}}(\text{HG}_0 + \text{HG}_1)$ and $\text{EPR}_1 = \frac{1}{\sqrt{2}}(\text{HG}_0 - \text{HG}_1)$. We have obtained $\langle \Delta^2(\hat{x}_0^{\text{EPR}} - \hat{x}_1^{\text{EPR}}) \rangle + \langle \Delta^2(\hat{p}_0^{\text{EPR}} + \hat{p}_1^{\text{EPR}}) \rangle = 2.51(6) < 4$ (the Duan entanglement criterion [33, 34]) and $\langle \Delta^2\hat{x}_{1|0}^{\text{EPR}} \rangle \langle \Delta^2\hat{p}_{1|0}^{\text{EPR}} \rangle = 0.71(4) < 1$ (the EPR criterion [35]). To prepare a linear cluster state, we use a basis of LC_k ($k = 0, 1, 2, 3$) which is obtained by applying a unitary matrix $U^{(\text{LC})}$ to the basis of HG_k ($k = 0, 1, 2, 3$), where

$$U^{(\text{LC})} = \begin{pmatrix} -0.344i & -0.421i & 0.531i & 0.650i \\ 0.344 & -0.765 & -0.531 & 0.119 \\ -0.765i & -0.344i & -0.119i & -0.531i \\ 0.421 & -0.344 & 0.650 & -0.531 \end{pmatrix}.$$

To check correlations among different modes, we use the four nullifiers associated with a linear cluster state [26, 36], $\hat{\delta}_k^{(\text{LC})} = \hat{x}_k - \sum_l V_{kl}\hat{p}_l$ (V_{kl} is the adjacency matrix defining the topology of a cluster state, where $V_{kl} = 1$ if k and l are connected, and 0 otherwise). They all exhibit a variance less than the vacuum fluctuation: $\langle \Delta^2\hat{\delta}_k^{(\text{LC})} \rangle / \langle \Delta^2\hat{\delta}_k^{(\text{LC})} \rangle_{\text{vacuum}} = 0.75(2), 0.67(2), 0.68(2)$, and $0.64(2)$ for $k = 0, 1, 2$, and 3 , respectively. Similarly, we prepare a square cluster state in the basis of SC_k ($k = 0, 1, 2, 3$), which is obtained by applying a unitary matrix $U^{(\text{SC})}$ to the HG basis, where

$$U^{(\text{SC})} = \begin{pmatrix} -0.316 & 0.632 & 0.707 & 0.000 \\ 0.632i & 0.316i & 0.000 & -0.707i \\ -0.316 & 0.632 & -0.707 & 0.000 \\ 0.632i & 0.316i & 0.000 & 0.707i \end{pmatrix}.$$

Each of the four nullifiers $\hat{\delta}_k^{(\text{SC})}$ associated with a square cluster state exhibits a variance less than the vacuum fluctuation: $\langle \Delta^2\hat{\delta}_k^{(\text{SC})} \rangle / \langle \Delta^2\hat{\delta}_k^{(\text{SC})} \rangle_{\text{vacuum}} = 0.72(2), 0.77(2), 0.61(2)$, and $0.75(2)$ for $k = 0, 1, 2$, and 3 , respectively.

Theoretical model. To calculate $\hat{\rho}^-$, we model a single-photon subtractor that takes into account experimental imperfections [27]:

$$\hat{\rho}^- = \mathcal{R}[\hat{\rho}] / \text{tr}[\mathcal{R}[\hat{\rho}]]; \quad \mathcal{R}[\hat{\rho}] = w_0\hat{\rho} + (1 - w_0)\mathcal{S}[\hat{\rho}], \quad (3)$$

where w_0 is the weight of background noise (e.g. dark counts) of the SPD which does not alter the input state. $\mathcal{S}[\hat{\rho}]$ is the actual photon subtraction from an input state:

$$\mathcal{S}[\hat{\rho}] = \frac{Np_0 - 1}{N - 1} \hat{A}\hat{\rho}\hat{A}^\dagger + \frac{1 - p_0}{N - 1} \sum_{k=0}^{N-1} \hat{a}_k \hat{\rho} \hat{a}_k^\dagger, \quad (4)$$

where N is the number of modes. \hat{A} is the desired photon subtraction in Eq. (1), whose weight is p_0 ; the remaining weight, $1 - p_0$, corresponds to the photon subtraction in

the incoherent mixture of the other modes with equal contribution. To consider the experimental conditions, we use $w_0 = 0.0094$, $p_0 = 0.95$, $N = 4$, and $\hat{\rho}$ in Extended Data Fig. 3. K_{ex} of $\hat{\rho}^-$ in a specific mode is then obtained by following the method presented in Refs. [23, 24], which is based on calculating multimode correlation functions.

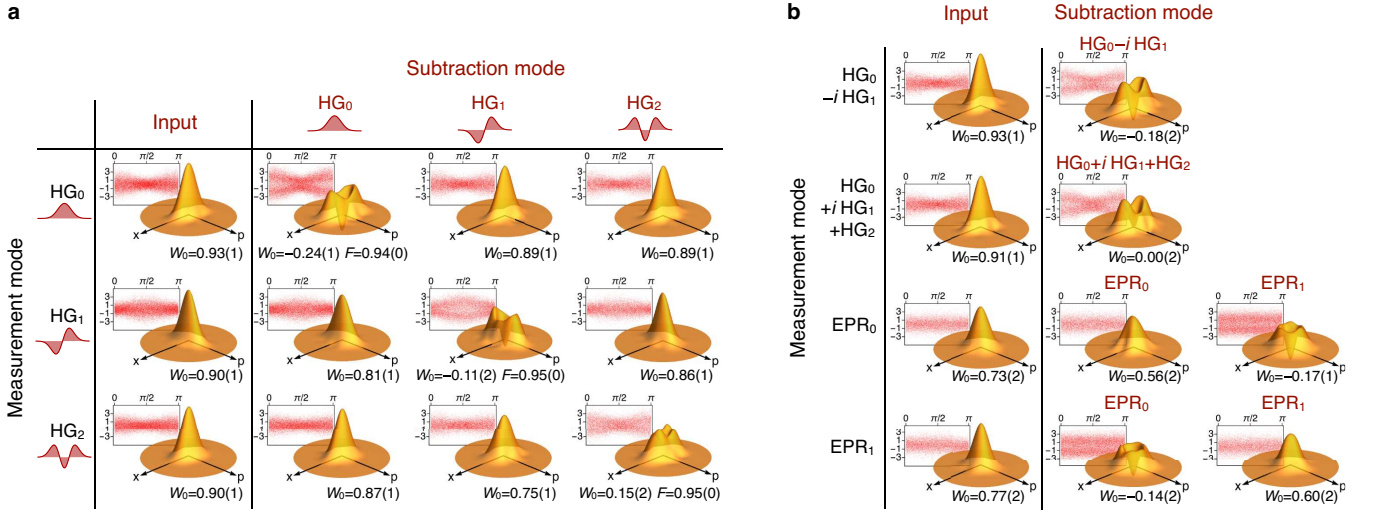
Negativity of a multimode Wigner function. A negative value in a single-mode Wigner function, which is reduced from a multimode Wigner function, is sufficient to show a negative value in the multimode Wigner function. The proof is straightforward by considering the contraposition of the statement: a non-negative multimode Wigner function always leads to a non-negative Wigner function when reduced to a single mode. Consider a reduced phase space \mathbb{R}^2 of an arbitrary single mode defining quadratures (x_0, p_0) and the entire phase space \mathbb{R}^{2N} of N modes defining quadratures $(x_0, p_0, \dots, x_{N-1}, p_{N-1})$. The Wigner function in the N modes is assumed to be non-negative: $W^{(N)}(x_0, p_0, \dots, x_{N-1}, p_{N-1}) \geq 0$. Then, the Wigner function in the reduced phase space $W(x_0, p_0)$ can be obtained by integrating the multimode Wigner function over the phase space of $(x_1, p_1, \dots, x_{N-1}, p_{N-1})$:

$$W(x_0, p_0) = \int_{\mathbb{R}^{2(N-1)}} dx_1 dp_1 \dots dx_{N-1} dp_{N-1} W^{(N)}.$$

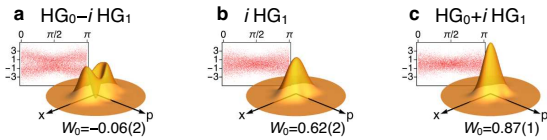
As $W^{(N)} \geq 0$, the reduced Wigner function $W(x_0, p_0)$ cannot have a negative value.

Measurement mode		Input	Subtraction mode		
			HG ₀	HG ₁	HG ₂
	HG ₀	0.91(1)	0.45(0) [0.53(2)]	0.88(1)	0.87(1)
	HG ₁	0.90(1)	0.82(1)	0.47(0) [0.49(1)]	0.86(1)
	HG ₂	0.91(1)	0.87(1)	0.77(1)	0.49(0) [0.50(2)]

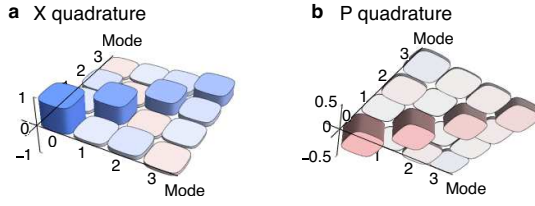
Extended Data Table 1. **Purities of the Wigner functions in Fig. 2(a).** For comparison, the purity of a Wigner function by the ideal photon subtraction is provided in square brackets, which agrees well with the experimental result. Low purity in a photon-subtracted mode is attributed to a non-ideal input state [18]. No optical loss is corrected in the calculation. Errors noted in parentheses are 1 s. d.



Extended Data Fig. 1. **Wigner function reconstructed with optical loss correction.** Optical loss in the homodyne detection (12.5%) has been corrected. Comparing with Fig. 2, non-Gaussian Wigner functions show reduced W_0 . Errors noted in parentheses are 1 s. d.



Extended Data Fig. 2. **Effect of mode mismatch between photon subtraction and measurement.** When a single photon is subtracted in $HG_0 - iHG_1$, a Wigner function (without optical loss correction) is obtained in a measurement mode having (a) full match ($HG_0 - iHG_1$), (b) partial match (iHG_1), and (c) no match ($HG_0 + iHG_1$). Errors noted in parentheses are 1 s. d.



Extended Data Fig. 3. **Experimental covariance matrix.** (a) is for x quadratures, seen from above, and (b) is for p quadratures, seen from below. Mode indexes are HG_0 , $i\text{HG}_1$, HG_2 , and $i\text{HG}_3$, where i is added for the odd-index HG modes to have p -squeezed vacua in all modes. For clarity, the vacuum noise (corresponding to the identity matrix) is subtracted from the covariance matrix. In the covariance matrix, variances of (x, p) quadratures are (2.8 dB, -1.8 dB) in mode 0, (2.1 dB, -1.6 dB) in mode 1, (1.6 dB, -1.0 dB) in mode 2, and (1.4 dB, -0.7 dB) in mode 3.